Astron. Astrophys. 313, 180–190 (1996)

ASTRONOMY
AND
ASTROPHYSICS

AGB stars: densities and formation rates obtained from OH/IR stars

R. Ortiz[1,2] **and W.J. Maciel**[2]

[1] Departamento de Fisica, UFES, Campus Universitario, 29060-900, Vitoria, ES, Brazil
[2] Instituto Astronômico e Geofísico da USP, Av. Miguel Stefano 4200, CEP 04301-904 São Paulo SP, Brazil

Received 26 May 1995 / Accepted 29 December 1995

Abstract. We determine densities and star formation rates of AGB stars from an analysis of OH/IR stars in the solar neighbourhood. The stars are divided into three distinct mass ranges corresponding to the precursors of type I, II and III planetary nebulae, according to the Peimbert classification scheme. The adopted distance scale is based on the period-luminosity relationship by Feast et al. (1989). The formation (or death) rates are calculated using stellar evolution models for AGB stars, and are compared with the corresponding rates for planetary nebulae and white dwarfs. The results indicate that both surface and volume densities of AGB stars are in good agreement with previous determinations in the literature. The formation rates are found to be very sensitive to the evolution time at the AGB, and depend also on the adopted model.

Key words: stars: AGB and post-AGB – stars: evolution – stars: circumstellar matter – ISM: planetary nebulae: general – Galaxy: solar neighbourhood – Galaxy: stellar content

1. Introduction

Since the work by Shklovskii (1956), asymptotic giant branch (AGB) stars are believed to be the precursors of planetary nebulae (PN). During the thermal pulse phase (TP-AGB), the star may experience a large mass-loss rate that contributes to the formation of a circumstellar dust shell (CDS). In oxygen-rich stars, the OH maser phenomenon occurs both in optically thick envelopes at the frequency of 1612 MHz (type II OH masers), and also in optically thin envelopes, at the frequencies of 1665 and 1667 MHz (type I OH masers). Carbon-rich stars may exhibit CO emission owing to transitions between rotationally excited levels.

Olnon et al. (1984) showed that Miras and OH/IR stars form a sequence in the IRAS color diagram $[12-25] \times [25-60]$. This has been interpreted as a sequence of increasing mass (and decreasing age) with the infrared color ([12-25], K-L, I-K, etc.), based on CDS models of (Lépine et al. 1995, hereafter LOE), and on the fact that redder stars are more concentrated on the galactic plane, showing smaller deviations from the galactic rotation curve (Ortiz & Maciel 1994, hereafter OM).

OM showed that OH/IR stars may be divided into classes resembling the PN types originally proposed by Peimbert (1978), regarding their scale heights, peculiar velocities, masses, and chemical abundances. The basic quantities used in the classification are the infrared colour indexes and the separation between the OH peaks, which is an indication of the expansion velocity of the envelope. A similar study has been conducted regarding visible Miras (Jura 1994, Jura & Kleinmann 1992, Jura et al. 1993). These stars have been described as a mixed population, using the periods as a classification parameter, in the sense that stars with longer periods are more concentrated on the galactic plane when compared to the shorter period ones. These studies were the first attempt to determine the densities of Miras taking into account their diversity in masses and ages.

Star formation rates (χ) at the various stages of stellar evolution are very useful in order to probe stellar evolution theories. The evaluation of χ for AGB stars, planetary nebulae, and white dwarfs is particularly important, as the transition through these different phases occurs in a very short time scale, during which the star preserves its spatial and kinematic properties. Thus, χ is expected to obey the continuity equation along the evolutionary track up to the point where the star becomes a white dwarf.

In this work, we determine the volume (ρ), and surface (or projected, σ) densities of AGB stars from a recently compiled catalogue of OH/IR stars that we believe to be complete up to $\sim$ 1 kpc from the Sun. We adopted the division of AGB stars into three classes (OM), which gives an indication of their masses (and ages). By using some recent synthetic models of AGB stars available in the literature, we derive the OH/IR ($\chi_{OH/IR}$) and AGB (χ_{AGB}) star formation rates for these classes, and compare them with the corresponding quantities for planetary nebulae (χ_{PN}) and white dwarfs (χ_{WD}).

Send offprint requests to: W.J. Maciel

2. The database

2.1. Completeness of the OH/IR catalogue

The database of the present study is a catalogue of OH/IR stars compiled from the literature. We consider as an OH/IR star any stellar infrared source at the AGB that emits OH maser at λ = 18 cm, with or without a visible counterpart. We do not distinguish between classical, visible Miras and infrared Miras, or OH/IR stars, since these objects are essentially the result of differing envelope optical depths. The distinction of these objects is therefore not well-defined, in the sense that a purely infrared source may have an optical counterpart, provided enough sensitivity is available. Moreover, both visible Miras and infrared OH/IR stars are TP-AGB stars, which differ only with respect to their masses (OM, LOE, Epchtein et al. 1990). This view is distinct from that proposed by van der Veen (1988), who argues that, as an AGB star evolves, it becomes redder until it undergoes the superwind phenomenon (Renzini 1981). According to this model, after a short period of intense mass-loss (the superwind), the star expels its envelope and becomes a planetary nebula.

We put together both type I and II OH masers, since we know that the emission comes from an AGB star. Objects such as supergiants and interstellar sources have been excluded. This is adequate, as visible Miras usually emit strongly in the frequencies of 1665 and/or 1667 MHz only, while infrared OH/IR stars emit predominantly in the 1612 MHz frequency. By including both types of maser emission, we make sure to cover the entire mass range for TP-AGB stars.

Since the original interpretation of maser phenomenon (Wilson & Barrett 1968), several surveys have been made, covering 1612, 1665, and 1667 MHz frequencies (sometimes also 1720 MHz). These include especially the Arecibo group (cf. Eder et al. 1988, Lewis et al. 1990, Chengalur et al. 1993, Lewis 1994), the Leiden group (cf. te Lintel Hekkert 1990, te Lintel Hekkert et al. 1991), and the Nançay group (cf. Likkel 1989, David et al. 1993a,b, Sivagnanam et al. 1988, Le Squeren et al. 1992). Such a variety of surveys permits us to assert that, at least for the solar neighbourhood, the sky coverage is complete both in direction and distance. The OH/IR star database used in the present work contains about 1700 objects, all of them with IRAS counterparts, representing 96 percent of the sky coverage. About 500 objects have near-infrared photometry available in the literature (J, H, K, L, and M photometric bands).

In order to determine the space density (ρ, kpc^{-3}), and the surface density (σ, kpc^{-2}) of OH/IR stars, we consider a cylinder centered at the Sun, with infinite height and with a well-determined radius. The determination of this limiting radius is essential for the completeness of the catalogue.

The two-micron sky survey (TMSS, Neugebauer & Leighton 1969) was the main database for several surveys of OH/IR stars until the advent of the IRAS survey in 1984. The TMSS is complete up to magnitude 3. Adopting for completeness a limiting distance of 1 kpc, we get an upper limit for the absolute magnitude $M_K = -7$, neglecting interstellar extinction. LOE present average absolute magnitudes for their infrared sequence of OH/IR stars, obtained by fitting a CDS model to the same catalogue used in this paper. They obtain M_K magnitudes brighter than -7 along their sequence of K-L colours up to K-L=2.7 However, at this colour the optical depth reaches $\tau(\lambda = 1\mu\text{m}) = 4.6$, which means that the CDS becomes optically thick, emitting radiation mainly in the mid and far-infrared, where the star can be detected by the IRAS satellite. At this point, the OH/IR star is purely infrared, i.e., it does not have a visible counterpart, unless the star is nearby, and its absolute magnitude at $\lambda = 12\mu$m is $M_{12} = -13$, which makes the star detectable up to several kpc from the Sun. Even towards those areas not covered by TMSS (for instance, below $\delta = -33°$), the IRAS catalogue is sensitive enough to detect any Mira within a 1 kpc radius. Sivagnanam et al. (1988) surveyed all Miras within a sphere with 1 kpc radius, and some stars beyond it, at the frequencies of 1612, 1665, and 1667 MHz. Despite the fact that their volume is a little different from ours, the space coverage is essentially the same, because the scale height of OH/IR stars H is less than 1 kpc. In fact, it depends on the mass of the precursor star, but $150 < H(\text{pc}) < 760$, within the complete sample of the present work.

The determination of densities and formation rates is very sensitive to the adopted distance scale, being proportional to the third and fourth power of the distances, respectively. The distances used in this work were derived from the period-luminosity relationship given by Feast et al. (1989), calibrated for oxygen-rich Miras in the Large Magellanic Cloud (LMC). When the period P of the star is unknown, it is estimated by means of a relationship between P and ΔV, the separation between the OH peaks (see OM and LOE for a detailed discussion). Although the use of the period-luminosity relationship may be considered suspect as applied to the Galaxy, owing to the metallicity difference between the LMC and the Galaxy, it has already been used successfully before (Whitelock et al. 1994). In fact, the dispersion in the period-luminosity relationship is about 0.15 magnitude, which can be considered as excellent for a distance scale. The interstellar extinction is treated as in OM and LOE, using a model that follows the atomic and molecular distribution of the gas (Ortiz & Lépine 1993, hereafter OL).

2.2. A catalogue of nearby OH/IR stars

Table 1 lists the OH/IR stars inside a cylinder with 1 kpc radius centered at the Sun, amounting to 76 objects. We list the IRAS name (column 1), the visible or near-infrared counterpart, if any (column 2), the period P (column 3), the distance D (column 4), and the height from the galactic plane $|z|$ (column 5). The last column gives the classification of the objects according to their [12-25] colour and ΔV as proposed by OM. For the 13 single peaked objects, we have taken into account in the classification the [12-25] colour and the period, which is related to ΔV. The main goal of the adopted classification is to identify the mass (age, metallicity) ranges of the progenitor stars, in order to obtain a more realistic picture of the mixed stellar population.

Table 1. Nearby OH/IR stars

IRAS name	Star	P (days)	D (kpc)	$\|z\|$ (kpc)	Class (OM)
00007+5524	Y Cas	413	0.65	0.07	III
01037+1219	WX Psc	660	0.77	0.59	I
01280+0237	R Psc	344	1.09	0.93	III
02168−0312	o Cet	331	0.11	0.09	III
02234−0024	R Cet	166	0.84	0.68	III
02522−5005	R Hor	407	0.40	0.34	III
03082+1436	U Ari	371	0.84	0.50	III
03336−7636	X Men	380	1.22	0.74	III
03507+1115	IK Tau	470	0.28	0.15	II
04094−2515	W Eri	376	0.94	0.67	III
04140−8158	U Men	-	0.46	0.25	III
04255+1033	R Tau	320	0.55	0.24	III
04355+0814	RX Tau	331	0.71	0.30	III
04387−3819	R Cae	391	0.54	0.36	III
05096−4834	S Pic	428	0.64	0.38	III
05098−6422	U Dor	394	0.76	0.44	III
05265−0443	S Ori	414	0.43	0.15	III
05450−3142	S Col	325	0.84	0.38	III
05528+2010	U Ori	368	0.26	0.01	III
06300+6058	TMSS +60169	-	0.87	0.32	II
06500+0829	GX Mon	527	0.93	0.07	III
07304−2032	Z Pup	508	0.87	0.01	III
07446−3210A	TMSS -30100	-	0.88	0.06	III
07585−1242	U Pup	318	0.64	0.10	III
08138+1152	R Cnc	361	0.29	0.12	III
09331−1428	X Hya	301	0.51	0.23	III
09425+3444	R LMi	372	0.44	0.34	III
09429−2148	IW Hya	636	1.03	0.41	II
09448+1139	R Leo	309	0.13	0.09	III
10133−5413	W Vel	394	0.60	0.02	III
10189−3432	V Ant	302	0.97	0.31	III
10580−1803	R Crt	-	0.30	0.18	III
11525−5057	-	-	0.96	0.18	III
12016+1903	R Com	362	1.16	1.13	III
12449+3838	U CVn	345	2.13	2.09	III
12562+2324	T Com	406	7.41	7.39	III
13462−2807	W Hya	-	0.10	0.05	III
14086−2839	RU Hya	331	0.80	0.41	III
14162+6701	U Umi	330	0.93	0.70	III
14247+0454	RS Vir	353	0.80	0.68	III
14559−5446	Y Lup	396	0.70	0.04	III
15193+1429	S Ser	371	1.34	1.06	III
15193+3132	S CrB	360	0.38	0.32	III
15255+1944	WX Ser	425	1.10	0.88	III
15262+0400	TMSS 00266	-	1.38	0.99	III
16081+2511	RU Her	484	0.94	0.67	III
16235+1900	U Her	406	0.40	0.26	III
17115−3322	RW Sco	389	0.72	0.04	III
17411−3154	AFGL 5379	-	0.90	0.02	I
17540−1919	VV Sgr	401	0.86	0.04	III
17541+1110	RT Oph	426	1.04	0.31	III
17574−2403	-	-	0.77	0.01	I
18009−2019	V4120 Sgr	-	0.84	0.01	II
18196−1331	-	-	0.95	0.00	II
18204−1344	-	-	0.64	0.00	III
18204−1344	-	-	0.86	0.00	II
18359+0847	X Oph	328	0.28	0.03	III
19039+0809	R Aql	284	0.27	0.00	III
19078+0901	-	-	0.87	0.00	I
19356+1136	RT Aql	327	0.64	0.05	III
19474−0744	GY Aql	-	0.56	0.16	III
19528−2919	RR Sgr	336	0.57	0.25	III
19550−0201	RR Aql	394	0.46	0.12	III
20015+3019	V719 Cyg	-	0.73	0.00	III
20047+1248	SY Aql	355	0.99	0.18	III
20077−0625	TMSS -10529	651	0.77	0.27	II
20255+3712	-	-	0.47	0.00	I
20259−4035	U Mic	334	0.93	0.53	III
21206−4054	V Mic	381	1.04	0.74	III
21286+1055	UU Peg	456	1.08	0.51	III
22516+0838	TMSS +10523	452	0.95	0.66	III
23041+1016	R Peg	378	0.56	0.39	III
23213−4521	NSV 14540	563	1.17	1.06	III
23412−1533	R Aqr	386	0.25	0.24	III
23425+4338	EY And	360	0.87	0.26	II
23558+5106	R Cas	430	0.18	0.03	III

We discarded two nearby supergiants (VY CMa and VX Sgr) inside the volume considered. There is one symbiotic star (R Aqr) that has been detected by Ivison et al. (1994). The star T Comae seems to have a poorly determined distance, which is probably due to the IRAS flux measurements. No infrared photometry has been published for this star, so that its distance can be considered as an upper limit. The IRAS source 18204-1344 is listed twice in the table, as it is identified with two distinct OH/IR stars in the same line of sight (cf. te Lintel Hekkert et al. 1989, Blommaert et al. 1994).

A rapid inspection of Table 1 reveals that the majority of the nearby OH/IR stars is classified as class III objects, that is, they have kinematic and spatial characteristics resembling those of type III planetary nebulae (Peimbert 1978, Maciel & Dutra 1992, Maciel & Köppen 1994). This class comprises stars near the lower limit of the intermediate mass range ($0.8 < M/M_{\odot} < 1.0$, OM). We see that 92 percent of class III OH/IR stars have a visible counterpart, i.e. are visible M-type Miras, 50 percent of class II OH/IR stars (four objects) have a visible counterpart, while only 20 percent of class I (one star) is identified with a visible Mira. This star (WX Psc) is an extremely red Mira (K-

Table 2. Scale heights and densities of OH/IR and AGB stars

Class	N	H (pc)	$\sigma_{OH/IR}$ (kpc^{-2})	$\rho_{OH/IR}$ (kpc^{-3})	σ_{AGB} (kpc^{-2})	ρ_{AGB} (kpc^{-3})	observed fraction
I	5	120	1.6	6.6	3.2	13.3	0.050
II	8	180	2.6	7.1	12.8	35.4	0.133
III	63	370	20	27	160	217	0.817
Total	76	330	24	41	176	265	1.000

L=2.52, Whitelock et al. 1994, [12-25]=1.367), with a period that may be considered long for a visible Mira (P=660 days), and ΔV = 36.4 km/s (Eder et al. 1988). Adopting the infrared sequence by LOE, the optical depth of its envelope is about $\tau(\lambda = 1\mu\text{m}) = 4.5$. The "visibility" of an OH/IR star therefore decreases as we consider classes in the order III, II, I, and the envelope becomes optically thick for class I objects.

Figure 1 shows the location of the OH/IR stars, projected onto the galactic plane, within 1 kpc radius, The Sun is at the centre of the figure, and the galactic centre is located to the right. Some interesting features can be observed in fig. 1: (i) no OH/IR stars are observed outside the solar circle; (ii) the distribution in longitude is approximately symmetric. This observation is important, as it indicates that both sky hemispheres are well covered by the surveys, in spite of the fact that the southern hemisphere is relatively less well studied. The lack of oxygen-rich stars outside the solar circle is consistent with previous studies showing that carbon stars become dominant for $R > R_0$ (Guglielmo 1993).

From the data of Table 1, we calculated the average scale height of each stellar type assuming an exponential distribution along the z-axis. The results for the three classes considered are shown in Table 2, where column 1 gives the class, column 2 the number of objects in a given class, and column 3 gives the scale height H. These results confirm that the adopted classification scheme is able to segregate stars according to their masses and ages. A similar conclusion was achieved by Jura (1994), Jura & Kleinmann (1992), and Jura et al. (1993), who studied M-type Miras segregating them according to their period. The results obtained by these authors (cf. Table 3) show that short-period ($P < 300$ days) M-type Miras have $H = 600$ pc; intermediate-period ($300 < P < 400$ days) objects have $H = 240$ pc, as well as the longest period ($P > 400$days) Miras. Therefore, a close correspondence between the classification proposed by OM and the period classification can be achieved. In the latter case, visible Miras were used and the obtained scale heights resemble those of class III and possibly some class II objects that exhibit a visible counterpart. We conclude that the period sequence as considered in the quoted papers is incomplete regarding the intermediate mass range of AGB stars, as it does not include the massive objects. These stars are essentially infrared objects, and can be observed mainly through infrared surveys.

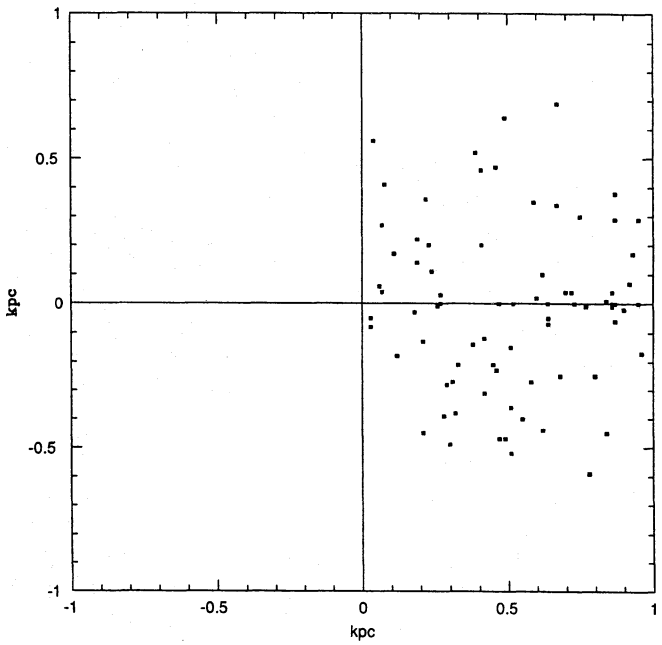

Fig. 1. Projected distribution of nearby OH/IR stars onto the galactic plane. The Sun is at the centre of the figure.

3. Densities of OH/IR and AGB stars

The stellar surface density can be easily determined, as can be seen from the projected distribution of fig. 1. This evaluation is quite reliable, as it does not depend on the adopted scale height, but only on the distance scale. The surface density σ for OH/IR stars can be determined for these objects from the relation $\sigma = N/\pi$, and is given in column 4 of Table 2.

The determination of the volume density ρ (kpc^{-3}) depends on the scale height. We calculated ρ from the surface density σ assuming that the vertical distribution of the stars can be described by an exponential law, so that

$$\sigma = \int_{-\infty}^{+\infty} \rho e^{-|z|/H}\, dz = 2\rho H \qquad (1)$$

The values of the volume density for OH/IR stars, $\rho_{OH/IR}$ are given in column 5 of Table 2. In order to determine the densities for AGB stars in general, some considerations have to be made on the frequency distribution of these stars as compared to OH/IR stars.

Table 3. Scale heights, surface and volume densities of AGB stars

Object	H (pc)	σ (kpc^{-2})	ρ (kpc^{-3})	Reference
Miras (all types)	315	154	245	Wood & Cahn (1977)
Short-period M-miras	600	42	35	Jura (1994)
Intermediate-period M-miras	240	100	210	Jura & Kleinmann (1992)
Long-period M-miras	240	18	38	Jura et al. (1993)
Carbon stars	200	40	100	Claussen et al. (1987)
Carbon stars	190	70	185	Groenewegen et al. (1992)
AGB stars (all types)	330	176	265	This work

Sivagnanam et al. (1988) searched for OH emission towards nearby ($d < 1$ kpc) visible Miras. The survey was made in three different frequencies of the $\lambda = 18$ cm ladder: 1612, 1665, and 1667 MHz. Three of their non-detections had positive results in other surveys: o Ceti (Dickinson et al. 1975), R Aqr (Ivison et al. 1994), and AU Cyg (Lewis 1994). After this small correction, we have for the volume considered N(non-OH)/N(OH)=3.00, which means that the OH maser phenomenon is rare, considering M-type Mira stars.

A quite different scenario is obtained when we look for OH emission towards purely infrared sources. Usually, 1612 MHz surveys are performed considering IRAS sources inside a well defined colour-box, which is characteristic of infrared, oxygen-rich AGB stars. Although different groups define their own colour-boxes, all of them define optically thick CDS's, which are more likely to present 1612 MHz emission. However, a very small number of objects is included in these colour-boxes that do not present the maser phenomenon. These are called colour-mimics, and a few studies tried to establish their nature. They could be symbiotic stars, in which the movement of the members, associated to the radiation pressure of the companion star, may destroy the coherent path necessary for the maser amplification (Seaquist & Ivison 1994, Lewis & Engels 1993). In fact, there are only two symbiotic stars (H1-36 and R Aqr) that exhibit the OH maser phenomenon, discovered in a specific survey (Ivison et al. 1994). Moreover, the number of colour-mimics is extremely low, less than 10 percent (Lewis & Engels 1993), so that these objects are neglected in this work.

We combined these different scenarios for the occurrence of maser emission in oxygen-rich AGB stars into our population of OH/IR stars. We corrected class III stars for the factor of ocurrence of OH masers in visible Miras found by Sivagnanam et al. (1988), since there is a close correspondence between their population and that considered in this study. Half of class II stars, which exhibit a visible counterpart, were corrected by the same factor, since this class includes a similar amount of visible and infrared OH Miras. Finally, class I objects were not corrected, since these objects are essentially infrared, resembling those objects defined in the infrared colour-boxes of the IRAS-PSC catalogue. The corrected surface and volume densities for oxygen-rich AGB stars are shown in Table 2, columns 6 and 7, respectively. Column 8 gives the observed fraction of each class, according to the catalogue data.

The chemical abundances depend on the location in the Galaxy. Radial abundance gradients have been determined for a variety of elements in planetary nebulae and HII regions (cf. Maciel & Köppen 1994, Maciel & Chiappini 1994). The C/O ratio depends on the space coordinates and on the evolution of the star, owing to the several dredge-up episodes the star experiences during the red giant phase (Iben & Renzini 1983). As a result, carbon becomes overabundant relative to oxygen in the outer Galaxy (Guglielmo 1993, Jura et al. 1989), while oxygen-rich stars are abundant inside the solar circle (Bowers 1978, Baud et al. 1981). The Sun occupies a strategic position that defines the loci of oxygen and carbon-rich stars (see fig.1). With the advent of high-sensitivity surveys in the CO transitions, and in the infrared (IRAS), the ratio of carbon to oxygen-rich stars has been better determined. Jura & Kleinmann (1989) estimate this ratio to be close to unity. A similar result was found by Zuckerman & Aller (1986), regarding carbon and oxygen abundances in planetary nebulae. These results suggest that the local number of AGB stars must be twice the number of OH/IR stars, which places the determination of σ(AGB) in good agreement with results found in the literature. This can be seen in Table 3, where we present some recent results on the scale heights, surface and volume densities of AGB stars. The last line reproduces our results from Table 2. The obtained volume densities are very close to that by Wood & Cahn (1977), and are consistent with other results found in the literature, if we assume that half of the Miras are oxygen-rich.

From Table 2, we note that about 82% of the sample are class III OH/IR stars, 13% class II objects, and 5% are more massive, class I objects. Therefore, we conclude that in the solar neighbourhood class I objects (precursors of nitrogen-enriched type I planetary nebulae) constitute a fairly rare event. The same result was found by Zijlstra & Pottasch (1991) for planetary nebulae: the majority of nearby planetary nebulae originate from old stars. The fact that we observe approximately equal proportions of types I, II, and III (see for instance Maciel & Dutra 1992) in a sample of well-studied planetary nebulae, is due to

Table 4. Parameters and results of the GJ model for AGB evolution.

$M/M_\odot$	Z	$t_M + t_S$ $\times 10^3$yr	t_C $\times 10^3$yr	t_{AGB} $\times 10^3$yr	ΔM ($M_\odot$)	$F(M)$	f_{M+S}	f_C	f_{AGB}
(1)	(2)	(3)	(4)	(5)	(6)	(7)	(8)	(9)	(10)
0.93	0.0020	231	0	231	0.80 – 0.96	0.1283	0.053	0.000	0.053
1.00	0.0037	160	0	160	0.96 – 1.08	0.0882	0.025	0.000	0.025
1.16	0.0058	142	83	225	1.08 – 1.18	0.0633	0.016	0.009	0.025
1.20	0.0062	138	103	241	1.18 – 1.25	0.0398	0.010	0.007	0.017
1.30	0.0068	288	0	288	1.25 – 1.35	0.0514	0.026	0.000	0.026
1.40	0.0072	299	28	327	1.35 – 1.45	0.0460	0.024	0.002	0.027
1.50	0.0076	294	68	362	1.45 – 1.75	0.1134	0.059	0.014	0.073
2.00	0.02	510	46	556	1.75 – 2.25	0.1357	0.123	0.011	0.134
2.50	0.02	691	162	853	2.25 – 2.75	0.0968	0.119	0.028	0.147
3.00	0.02	866	260	1126	2.75 – 5.00	0.2370	0.364	0.109	0.474
					Total:	1.0000	0.820	0.180	1.000

a selection effect, in the sense that type I planetary nebulae are usually brighter than type III (Schönberner 1983, Cazetta & Maciel 1994), which makes the former detectable even at large distances.

4. Formation rates

In order to determine the formation rates for OH/IR stars and AGB stars in general we need, besides the volume densities given in Table 2, an estimate of the characteristic times spent in these phases, as given by recent evolution models for AGB stars. The evolution of a star on the AGB has become better understood with the advent of detailed physical models (cf. Renzini & Voli 1981). The dredge-up processes are specially important for the chemical evolution of the stellar atmosphere, and, due to the strong mass-loss during the AGB phase, also for the chemical evolution of the Galaxy (Matteucci & François 1989).

The third dredge-up process that occurs at the TP-AGB phase is particularly interesting for the present work, as it determines the spectral classification of the star: M-type (oxygen-rich, OH/IR), S-type (C/O = 1), or C-type (carbon-rich star). It is not clear whether all AGB stars will experience this dredge-up, or only those that are more massive.

Recently, Groenewegen & de Jong (1993, hereafter GJ) proposed a synthetic TP-AGB model in order to explain this phase of stellar evolution. Their model predicts the photospheric abundances and the time spent in each evolutionary phase, as well as other physical parameters such as luminosities, mass-loss, etc. The model can successfully explain these characteristics for stars in the LMC. In this work, we apply their grid of models to the OH/IR star population in the solar neighbourhood, in order to calculate the formation rates of OH/IR and other AGB stars. Although the model was not designed for the Galaxy, it is expected to produce reasonable results along the AGB mass sequence as considered in this article.

More recently, Groenewegen et al. (1995, hereafter GHJ) have proposed a revised evolutionary scenario for carbon stars in the solar neighbourhood. They have also determined lifetimes for the main phases of AGB evolution. These models are more appropriate for the discussion in the present paper, so that they have also been taken into account.

Finally, in order to compare our results with other independent models, we have also considered the model by Vassiliadis & Wood (1993, hereafter VW). Some different hypotheses are made, such as the introduction of a "superwind" at the end of the AGB as a deviation of the Reimers's formula for mass-loss. The application of two distinct models to the same population of stars is expected to have some influence on the star formation rates, so that we may have an opportunity to select among these models.

4.1. The Groenewegen & de Jong (GJ) model

In the following, we will apply the GJ models in order to determine the characteristic AGB times. For a detailed description of the models, we refer the reader to the original papers (GJ, Groenewegen & de Jong 1994a,b,c).

We adopt a grid of models appropriate for the Galaxy on the basis of the metallicity and mass-loss rates. The grid of models was extracted from Table 5 of GJ, and is displayed in our Table 4. The sequence of increasing metallicities indicates a decreasing sequence of age, as expected from the mass sequence. Column 1 of Table 4 gives the model initial mass $M/M_\odot$; column 2 gives the metallicity Z; column 3 shows the times spent as M and S spectral types ($t_M + t_S$); column 4 gives the duration of the C-rich phase (t_C), and column 5 gives the total AGB time (t_{AGB}).

The TP-AGB model alone is unable to reproduce the sequence proposed. We must mix the models of the grid at the exact proportions in order to simulate the mass distribution in the solar neighbourhood. We adopt the initial mass function (IMF) given by Miller & Scalo (1979) to obtain the correct mass proportions. It is obvious that the IMF is different from the present-day mass function (PDMF), but the *shape* of these functions does not change appreciably even if we take into account very different birthrates along the history of the Galaxy.

Table 5. Parameters and results of the GHJ model for AGB evolution.

$M/M_\odot$	Z	$t_M + t_S$ $\times 10^3$yr	t_C $\times 10^3$yr	t_{AGB} $\times 10^3$yr	ΔM $(M_\odot)$	$F(M)$	f_{M+S}	f_C	f_{AGB}
(1)	(2)	(3)	(4)	(5)	(6)	(7)	(8)	(9)	(10)
0.97	0.0008	486	0	486	0.80 – 0.98	0.1436	0.107	0.000	0.107
1.00	0.0033	206	0	206	0.98 – 1.10	0.0861	0.027	0.000	0.027
1.20	0.0107	281	0	281	1.10 – 1.30	0.1162	0.050	0.000	0.050
1.40	0.0171	358	0	358	1.30 – 1.42	0.0576	0.032	0.000	0.032
1.45	0.0178	359	28	386	1.42 – 1.47	0.0219	0.012	0.001	0.013
1.50	0.0181	356	52	407	1.47 – 1.55	0.0328	0.018	0.002	0.020
1.60	0.0182	354	106	460	1.55 – 1.67	0.0447	0.024	0.007	0.031
1.75	0.0183	354	204	558	1.67 – 1.87	0.0647	0.035	0.020	0.055
2.00	0.0185	443	310	753	1.87 – 2.25	0.0983	0.067	0.046	0.113
2.50	0.0188	442	773	1214	2.25 – 2.75	0.0968	0.066	0.114	0.180
3.00	0.0189	622	1001	1623	2.75 – 3.25	0.0735	0.070	0.113	0.183
3.50	0.0191	225	746	971	3.25 – 3.75	0.0583	0.020	0.067	0.087
4.00	0.0191	138	537	675	3.75 – 4.50	0.0684	0.014	0.057	0.071
5.00	0.0191	552	0	552	4.50 – 5.00	0.0368	0.031	0.000	0.031
					Total:	1.0000	0.573	0.427	1.000

The IMF is normalized to unity in the mass range:

$$\int_{0.8}^{5.0} M\phi(M)\,dM = 1 \qquad (2)$$

where M is the stellar mass and $\phi(M)$ is the IMF, which can be fitted by a power-law expression:

$$\phi(M) = \begin{cases} 0.7606 \times M^{-1.4} & \text{if } 0.8 < M/M_\odot < 1.0 \\ 0.7606 \times M^{-2.5} & \text{if } 1.0 < M/M_\odot < 5.0. \end{cases} \qquad (3)$$

OH/IR and carbon stars, as well as planetary nebulae, have progenitor star masses between $0.8 < M/M_\odot < (5-8)$. The upper limit is uncertain but this does not sensibly affect our results. The limit of 5 solar masses was chosen due to the fact that this value is closer to the higher mass of the grid. For each model, we integrated IMF in the mass intervals ΔM given in column 6 of Table 4. The integrated values $F(M)$ are given in column 7 of this table.

The relative number of AGB stars in each mass range is proportional to the time spent in this phase, as given in columns 3, 4, and 5 of Table 4, and to the relative number of stars in the respective mass range, as given in column 7 of this table. The product of these two quantities, renormalized to the unity, gives the fraction f of stars in a given phase, and is shown in columns 8, 9, and 10 of Table 4 for the phases M+S, C and AGB, respectively.

An analysis of the results given in Table 4 allows some conclusions to be drawn:

First, it can be seen that the average times on the AGB *increase* as the initial mass increases, a result that is not observed in other models for AGB stars (cf. Sects. 4.2 and 4.3).

Second, from the last column of Table 4, we see that the GJ models predict that about 50% of the AGB stars should have $M > 2.7 M_\odot$. This is in disagreement with the observations as given in our Table 2, where we note that the fraction of massive, class I AGB stars is about 5%. This discrepancy could be explained if the lifetimes of the massive stars are overestimated by the model.

Third, according to the GJ models, the ratio of C stars to the oxygen rich stars is about 0.18/0.82 = 0.22, from the last column of Table 4. Since the observed fraction is close to unity (cf. Zuckerman & Aller 1986, Jura & Kleinmann 1989), the GJ models show a strong deficiency of C stars. This can possibly be due to metallicity effects, as the GJ models are primarily intended for the LMC objects.

Let χ_{AGB} be the formation rate (kpc^{-3}) for AGB stars. If we assume that every TP-AGB star becomes a planetary nebula (Schönberner 1983), we can write the continuity equation:

$$\chi_{PN} = \chi_{AGB} = \left(\frac{\rho}{t}\right)_{AGB} \qquad \text{kpc}^{-3}\text{yr}^{-1}. \qquad (4)$$

Adopting the OM classification, eq. (4) can be more correctly written as:

$$\chi_{AGB} = \left[\left(\frac{\rho}{t}\right)_I + \left(\frac{\rho}{t}\right)_{II} + \left(\frac{\rho}{t}\right)_{III}\right]_{AGB} \qquad \text{kpc}^{-3}\text{yr}^{-1}. \qquad (5)$$

The volume densities of the AGB classes are given in Table 2. In order to obtain the characteristic times for the GJ models, we have to assign mass intervals to the different AGB stars. This is rather uncertain, especially since some overlapping may occur in the different classes. Taking into account the original proposal for the Peimbert classification system of planetary nebulae (Peimbert 1978), as well as more recent developments (Faúndez-Abans and Maciel 1986; Maciel and Köppen 1994), we adopt for the progenitor stars:

Class III $\quad 0.8 < M(M_\odot) < 1.1$

Class II $\quad 1.1 < M(M_\odot) < 2.2$

Class I $2.2 < M(M_\odot) < 5.0$

so that, for the purposes of the present work, we may write for the average masses of the different OM types: $M(III) \simeq 1.0M_\odot$; $M(II) \geq 1.0M_\odot$, and $M(I) \geq 1.4M_\odot$. Therefore, from Table 4 we have the following AGB times: $t_{AGB}(III) \simeq 2 \times 10^5$ yr; $t_{AGB}(II) \geq 2 \times 10^5$ yr, and $t_{AGB}(I) \geq 3 \times 10^5$ yr. In this case, class III dominates in eq. (5), so that we have

$$\chi_{AGB} \simeq \left(\frac{\rho}{t}\right)_{III} \quad (6)$$

that is, most of the newly-formed AGB stars are objects near the lower limit of mass. Using our result of Table 2, $\rho_{III} = 217\mathrm{kpc}^{-3}$, we get $\chi_{AGB} = 1.1 \times 10^{-3}\mathrm{kpc}^{-3}\mathrm{yr}^{-1}$. This result is close to those found for PN by Alloin et al. [1976, $\chi_{PN} = (0.63-3.1)\times 10^{-3}\mathrm{kpc}^{-3}\mathrm{yr}^{-1}$] and Tinsley (1978, $\chi_{PN} = 1.2 \sim 4.8 \times 10^{-3}\mathrm{kpc}^{-3}\mathrm{yr}^{-1}$), but is lower than the majority of results compiled by Maciel (1989) and Phillips (1989) by a factor two. Wood & Cahn (1977) studied visible Miras of all spectral types and found $\chi = 0.3 \times 10^{-3}\mathrm{kpc}^{-3}\mathrm{yr}^{-1}$, a very low value, when compared to planetary nebulae, although they found a result for the density very similar to ours. This discrepancy suggests that the calculus of χ is very uncertain due mainly to the poor knowledge of t_{AGB}, despite the efforts made in this field.

4.2. The Groenewegen et al. (GHJ) model

In order to derive results that are more appropriate to galactic objects, we have also taken into account the models by Groenewegen et al. (1995), as given in Table 5. This table has the same quantities of Table 4, and was based on Table 2 of GHJ. Groenewegen et al. (1995) presented two grids of models, considering (a) Reimers (1975) mass loss law with a scale factor $\eta = 4$, and (b) the recent mass loss law by Blöcker & Schönberner (1993, hereafter BS), with a scale factor $\eta = 0.08$. For the sake of simplicity, we have adopted here the GHJ results for Reimers' law, and discussed the effects of the BS law where appropriate.

The determination of the quantities $F(M), f_{M+S}, f_C$ and f_{AGB} followed the same steps as in Sect. 4.1. Similarly, some conclusions can also be drawn for the GHJ models:

First, the average AGB times increase up to $3M_\odot$, decreasing for large masses as in the models by Vassiliadis & Wood (1993, see next section). This effect is even more pronounced for the BS models.

Second, from Table 5 the expected fraction of AGB stars with $M > 2.7M_\odot$ drops to about 37%, both for Reimers and BS mass loss laws. This is lower than for the GJ models, but still much higher than our observed result of about 5%. Therefore, the decreased lifetimes of these massive stars in the GHJ models are not sufficient to explain the observations, so that they can still be considered as upper limits, especially in the range $2.5 - 3.0M_\odot$.

Third, the ratio of C stars to oxygen rich stars increases in the GHJ models to 0.75. This rate is about 0.9 for the BS models. This result is much closer to the observed fraction than in the GJ models, confirming our suggestion that the latter are not particularly appropriate for the galactic objects. However, it should be stressed that this ratio is not well determined, and there are suggestions which encompass a range of $0.2 < \mathrm{C/M} < 0.9$. GHJ seem to favour ratios close to the lower limit, whereas our own estimate based on their data gives a ratio of about $0.7 - 0.9$. As seen in Sect. 4.1, this procedure applied to the GJ models gives C/M = 0.2, clearly showing that there is some discrepancy between the GJ and GHJ models. This discrepancy probably derives from the adopted mass range for carbon stars, which is limited to the large mass objects, according to GHJ. Since carbon Miras are observed with optically thin CDE, some of these objects are probably low mass stars. Therefore, a detailed study of the space distribution of C stars is needed, in order to clarify the question of the mass distribution of these stars.

Finally, the average AGB times for the different OM types are similar to the results of Sect. 4.1, especially for stars of masses $M < 2M_\odot$. This is true except for the less massive stars, $M < 1M_\odot$. Therefore, the formation rates for the GHJ models are slightly lower than the corresponding rates for the GJ models, $\chi_{AGB} \simeq \chi_{AGB}(III) = 0.5 \times 10^{-3}\mathrm{kpc}^{-3}\mathrm{yr}^{-1}$.

4.3. The Vassiliadis & Wood (VW) model

Vassiliadis & Wood (1993) published a series of models of stellar evolution from the main sequence to the TP-AGB and beyond. The calculations were performed for several stellar masses and metallicities, and the results predict for each phase the lifetimes, luminosities, periods, as well as abundances of He and CNO elements. However, they do not give explicitly in their paper the time spent in the oxygen and carbon-rich phases. Also, the mass-loss is taken into account in a somewhat different way: a superwind phase is invoked, at the end of the TP-AGB phase in order to expel the stellar envelope. Such phenomenon is adopted in order to obtain mass-loss rates much higher than those given by Reimers (1975) formula. If the superwind exists is a matter of controversy, but following the point of view that a sequence of mass corresponds to a sequence of colour index or envelope optical depth, the superwind would cause a sudden change of the characteristics of the circumstellar dust shell (CDS). Such modification would change the color of a intermediate mass star into an extremely red star, due to the increasing optical depth of the envelope. As we stressed in this paper, the observations indicate that redder stars are intrinsically younger than the bluer ones. An alternative interpretation given by VW is that, while the superwind phase is about 10 percent of the TP-AGB lifetime of a 1 solar mass star, it can reach almost the entire lifetime of the TP-AGB phase for a intermediate mass star. We shall consider in this work both cases separately.

Table 6 is built similarly to Tables 4 and 5, but listing explicitly t_{AGB} and t_{SW}, the total-AGB and superwind lifetimes, respectively. The columns give: the initial mass $M/M_\odot$ (column 1); the metallicity Z (column 2); the time spent on the main sequence t_{MS} (column 3); the time during which the star remains visible t_{opt}, that is, the envelope is optically thin (column 4); the superwind time t_{SW} (column 5); the total AGB time t_{AGB} (column 6); the mass range considered for the integration

Table 6. Parameters and results of the VW's model for AGB evolution.

$M/M_\odot$	Z	t_{MS} $\times 10^9$yr	t_{opt} $\times 10^3$yr	t_{SW} $\times 10^3$yr	t_{AGB} $\times 10^3$yr	ΔM ($M_\odot$)	$F(M)$	f_{SW}	f_{AGB}
(1)	(2)	(3)	(4)	(5)	(6)	(7)	(8)	(9)	(10)
1.0	0.016	11.25	434.	61.	495.	0.80 – 1.25	0.3196	0.023	0.184
1.5	0.016	2.74	729.	98.	827.	1.25 – 1.75	0.2107	0.024	0.203
2.0	0.016	1.24	1060.	120.	1175.	1.75 – 2.25	0.1357	0.019	0.185
2.5	0.016	0.62	2070.	110.	2184.	2.25 – 3.00	0.1359	0.017	0.345
3.5	0.016	0.23	297.	130.	427.	3.00 – 4.00	0.1178	0.018	0.059
5.0	0.016	0.10	142.	120.	262.	4.00 – 5.00	0.0804	0.011	0.025
						Total:	1.0000	0.112	1.000

of the IMF, ΔM (column 7); the integrated IMF, $F(M)$ obtained as in the GJ and GHJ cases (column 8); the fraction of stars at the superwind phase in the corresponding mass range f_{SW} (column 9), and the fraction of stars at the AGB phase f_{AGB} (column 10).

Considering now the results of Table 6, some conclusions can also be drawn, as in the case of the previous models:

First, the average AGB times have a different behaviour as compared with the GJ models, in the sense that these times are larger for the low and intermediate mass objects (roughly corresponding to our class III and II objects), but decrease for the larger mass stars (roughly corresponding to our class I stars). This behaviour is closer to the GHJ models, as seen in Sect. 4.2.

Second, Table 6 shows that about 8% of the AGB stars have $M > 3.0M_\odot$, which is similar to our result that about 5% of these stars are class I. However, the VW models still predict a relatively large fraction of stars with $M \geq 2.2M_\odot$, namely 43%. This is probably due to the extremely large lifetimes predicted by the VW model for this mass interval. In order to completely reconcile our result with the models of Table 6, we would have to extend our class III up to 3.0 solar masses, which is incompatible with the scale heights and peculiar velocities found for AGB stars by OM.

Let us now determine the formation rate χ_{AGB} on the basis of the results of Table 6. Adjusting the mass intervals as $M/M_\odot \simeq 1.0$ (class III), $1.0 < M/M_\odot < 3.5$ (class II), and $2.0 < M/M_\odot < 5.0$ (class I), we obtain $t_{AGB}(III) \simeq 5 \times 10^5$ yr; $4.3 \times 10^5 < t_{AGB}(II)$ (yr) $< 2.2 \times 10^6$, and $2.6 \times 10^5 < t_{AGB}(I)$ (yr) $< 2.2 \times 10^6$, so that we have with the volume densities given in Table 2: $\chi_{AGB}(III) \simeq 0.43 \times 10^{-3}$kpc^{-3}yr^{-1}, $0.02 \times 10^{-3} < \chi_{AGB}(II)$(kpc^{-3}yr^{-1}) $< 0.08 \times 10^{-3}$, and $0.006 \times 10^{-3} < \chi_{AGB}(I)$(kpc^{-3}yr^{-1}) $< 0.05 \times 10^{-3}$. Therefore, approximation (6) still holds in this case, so that the total AGB formation rate is $\chi_{AGB} \simeq 0.4 \times 10^{-3}$kpc^{-3}yr^{-1}. This is very close to the earlier result by Wood and Cahn (1977) for Mira stars, $\chi_M = 0.3 \times 10^{-3}$kpc^{-3}yr^{-1}. Taking together the models of this and the preceding section, we have for the formation rate of AGB stars

$$\chi_{AGB} \simeq (0.4 - 1.1) \times 10^{-3}\text{kpc}^{-3}\text{yr}^{-1} \quad (7)$$

An upper limit for χ_{AGB} can be obtained if we consider the characteristic time of the *superwind* phase $t_{SW} \simeq 6 \times 10^4$ yr in eq. (6) instead of t_{AGB}. We have then $\chi_{AGB} < 3.6 \times 10^{-3}$kpc^{-3}yr^{-1}. Therefore, we can combine this result with the previous range for χ_{AGB} and write

$$0.4 \times 10^{-3} < \chi_{AGB}(\text{kpc}^{-3}\text{yr}^{-1}) < 3.6 \times 10^{-3}. \quad (8)$$

This range is in good agreement with the recent determinations for PN as given by Maciel (1989) and Phillips (1989). Also, in a recent analysis of the PN formation rate from a sample of objects with individual distance determinations, Pottasch (1995) obtains $\chi_{PN} = 3 \times 10^{-3}$ kpc^{-3} yr^{-1}, which is close to the upper limit of (8). It should be recalled that the PN formation rate may be strongly affected by the uncertainties in the PN distance scale, which also affects the individual distance determinations, so that we can consider our result (7) (or even eq. 8) as a very good agreement with our current knowledge of the evolution of intermediate mass stars. On the other hand, we stress that our result is basically affected by the determination of the characteristic time t_{AGB}, apart from the adopted distance scale.

If we recall the continuity equation between the AGB and the planetary nebula phases as given in eq. (4), we get a constraint for stellar evolution theories. Taking $\chi_{PN} = 2.5 \times 10^{-3}$kpc^{-3}yr^{-1} as a representative value from the compilations by Maciel (1989) and Phillips (1989), and $\rho \simeq 217$kpc^{-3} (Table 2), we obtain $t_{AGB}(III) \simeq 8.7 \times 10^4$ yr, which corresponds to the AGB lifetime for stars near $0.8 \sim 1.0M_\odot$.

4.4. The white dwarf connection

White dwarf densities and formation rates are extremely difficult to determine, due to strong selection effects. On the other hand, their lifetime t_{WD} is more reliable than t_{AGB}, since it depends on the star cooling rate, which is better known. Despite these difficulties, white dwarfs constitute an important clue in understanding the AGB-PN-WD evolution. Most estimates of χ_{WD} are in the range $1.4 - 2.5 \times 10^{-3}$kpc^{-3}yr^{-1} (Phillips 1989, Weidemann 1991), which is similar to, or lower than, the average value estimated for planetary nebulae.

According to Phillips (1989), if most white dwarfs with $M_{WD} > 0.55M_\odot$ are assumed to derive from planetary nebulae, then $\chi_{PN} = 0.6\chi_{WD}$, which is in good agreement with most estimates of χ_{PN} found in the literature. However, an earlier estimate by Fleming et al. (1986) gives $\chi_{WD} \simeq (0.49 -$

$0.75) \times 10^{-3}\mathrm{kpc}^{-3}\mathrm{yr}^{-1}$, which is much lower than χ_{PN}. If this value is correct, this could become a difficult problem to solve, involving reviewing distance scales, etc. From our eq. (7) it can be seen that their value of χ_{WD} is compatible with our determination of χ_{AGB}. χ_{WD} is probably lower than χ_{AGB}, as white dwarfs may originate from low-mass stars, that do not experience the TP-AGB ascension. They leave their envelopes at the RGB and early-AGB phases, evolving directly to the white dwarf phase, without any trace of a planetary nebula around it. The comparison of χ_{AGB} and χ_{WD} seems to confirm the result by Fleming et al. (1986); moreover if $\chi_{PN} = \chi_{AGB} = 0.6\chi_{WD}$, then the estimate of t_{AGB} form the GJ models seems to be more accurate.

5. Total numbers and birthrate in the Galaxy

The total number of AGB stars and their formation rates are important to understand the chemical evolution of the Galaxy, and the physics of the interstellar medium. Since these objects are intrisically bright ($10^4 - 10^5 L_\odot$) they can be detected even at distant regions like the bulge. However, strong selection effects do not permit us to know the real luminosity function of these objects in the whole Galaxy. Usually, the mass and luminosity functions and the formation rates are extrapolated for other parts of the Galaxy from their values in the solar neighbourhood. This is done by means of galactic structure models that try to reproduce the galactic mass distribution, star counts, and brightness distribution.

Models designed for the infrared region of the spectrum are of special interest here, because they provide the best fitness to the distribution of bright infrared objects, like AGB stars. Eaton et al. (1984), Garwood & Jones (1987), Guglielmo (1990), Ruelas-Mayorga (1991a,b), Wainscoat et al. (1992), and OL propose galactic models specially designed for the infrared, consisting of several mixed populations with different distributions and ages. OL propose a model that consists of a spheroidal component, two disk components with scale heights 100 and 390 pc, and a spiral-arm structure. The splitting of the disk population into two distinct distributions with different scale heights is similar to the treatment of the AGB mass sequence in this paper. The young disk (H=100 pc) consists of more massive stars (like class I OH/IR stars), while the old one (H=390 pc) is very similar to the distribution of class III OH/IR stars.

In Sect. 4 we concluded that the majority of AGB stars have relatively low-mass progenitors (cf. Zijlstra & Pottasch 1991). Since this population is dominant, we adopt the scale length of the thick disk α = 2.6 kpc, which is shorter than the value found by Bahcall & Soneira (1980) for the visible (α = 3.5kpc). All models designed for the infrared use values of α lower than those designed for the visible, with the exception of the model by Wainscoat et al. (1992), that assumes the scale length by Bahcall & Soneira (1980). Besides, the model by OL proved to be successful also to determine the galactic rotation curve (Amaral et al. 1995), by taking into account both AGB stars and planetary nebulae.

The total number of OH/IR stars and/or AGB stars may be calculated by direct integration:

$$N = 2\pi \int_0^{R_f} \sigma(r) r\, dr = 2\pi\sigma_0 \int_0^{R_f} \exp\left[\frac{-(r-R_0)}{\alpha}\right] r\, dr \quad (9)$$

where we have made explicit that σ_0 is the local density of stars, α is the scale lenght of the disk, R_0 refers to the solar neighbourhood, and R_f the radius of the Galaxy. The choice of R_f depends strongly on the abundances considered. As we mentioned earlier, OH/IR stars become rare outside the solar circle, whereas carbon stars are dominant. On the other hand, the sum of oxygen and carbon-rich stars constitutes a more continuous distribution; in this case, the integral must be performed up to several kpc beyond R_0.

For AGB stars equation (9) becomes:

$$N = 2\pi\sigma_0\alpha^2 e^{R_0/\alpha} \quad (10)$$

while for OH/IR stars, adopting $R_f \simeq R_0$:

$$N \simeq 2\pi\sigma_0\alpha\left[\alpha\left(e^{R_0/\alpha} - 1\right) - R_0\right] \quad (11)$$

Adopting α = 2.6 kpc, R_0 = 7.9 kpc (OL), and the σ_0 values shown in Table 2 we get: $N_{AGB} = 1.6 \times 10^5$, and $N_{OH/IR} = 1.7 \times 10^4$.

It is interesting to note that, until now, about 1700 OH/IR stars were detected. Despite the fact that they are very luminous in the radio and infrared domains, we have detected just about one-tenth of the existing OH/IR stars in the Galaxy, due to selection effects. Considerable efforts must be made to detect less-luminous OH/IR stars, mainly towards the bulge and beyond, by means of high-sensitivity and spatial resolution scans.

Our estimate for N_{AGB} permits to obtain the birthrate (yr^{-1}) for the whole Galaxy. Assuming the approximation given by equation (6), we have:

$$\begin{aligned} N/t_{AGB} &\simeq 0.8\mathrm{yr}^{-1} \quad (GJ) \\ N/t_{AGB} &\simeq 0.3\mathrm{yr}^{-1} \quad (GHJ) \\ N/t_{AGB} &\simeq 0.3\mathrm{yr}^{-1} \quad (VW) \\ N/t_{AGB} &\leq 2.7\mathrm{yr}^{-1} \quad (VW, SW) \end{aligned}$$

A comparison between these results with those compiled by Phillips (1989) for planetary nebulae confirms the upper limit as given by the SW characteristic time. Adopting the TP-AGB lifetimes by GJ we get χ_{AGB} close to the value found for χ_{PN} by Alloin et al. (1976, $\chi_{PN} = 0.5 - 1.1\ \mathrm{yr}^{-1}$), Maciel (1981, $\chi_{PN} = 1.0\,\mathrm{yr}^{-1}$), Daub (1982, $\chi_{PN} = 0.7\,\mathrm{yr}^{-1}$), and Isaacman (1983, $\chi_{PN} = 1.0\,\mathrm{yr}^{-1}$). On the other hand, the adoption of the TP-AGB lifetime by VW leads to χ_{AGB} close to the results by Cahn & Wyatt (1978, $\chi_{PN} = 0.3 - 0.7\ \mathrm{yr}^{-1}$), and Pottasch (1984, $\chi_{PN} = 0.1 - 0.3\ \mathrm{yr}^{-1}$). Again, the formation rates have shown to be strongly dependent on stellar evolution theories. We emphasize the importance of developing models that take

into account the AGB, planetary nebula, and the white dwarf phases, in order to obtain self-consistent results.

Acknowledgements. This work was partially supported by CNPq and FAPESP.

References

Alloin, D., Cruz-Gonzalez, C., Peimbert, M., 1976, ApJ 205, 74

Amaral, L.H., Ortiz, R., Lepine, J.R.D., Maciel, W.J., 1995, MNRAS (submitted)

Bahcall, J.N., Soneira, R.M., 1980, ApJS 44, 73

Baud, B., Habing, H.J., Matthews, H.E., Winnberg. A., 1981, A&A 95, 156

Blommaert, J.A.D.L., van Langevelde, H.J., Michiels, W.F.P., 1994, A&A 287, 479

Blöcker, T., Schönberner, D., 1993, in IAU Symp. 155, ed. R. Weinberger, A. Acker, Kluwer, Dordrecht, p. 479 (BS)

Bowers, P.F., 1978, A&A 64, 307

Cahn, J.H., Wyatt, S.P., 1978, in IAU Symp. 76, ed. Y. Terzian, Reidel Dordrecht, p.3

Cazetta, J., Maciel, W.J. 1994, A& A 290, 936

Chengalur, J.N., Lewis, B.M., Eder, J., Terzian, Y., 1993, ApJS 89, 189

Claussen, M.J., Kleinmann, S.G., Joyce, R.R., Jura, M., 1987, ApJS 65, 385

Daub, C.T., 1982, ApJ 260, 612

David, P., Le Squeren, A.M., Sivagnanam, P., Braz, M.A., 1993a, A&AS 98, 245

David, P., Le Squeren, A.M., Sivagnanam, P., 1993b, A&A, 277, 453

Dickinson, D.F., Kollberg, E., Yngvesson, S., 1975, ApJ 199, 131

Eaton, N., Adams, D.J., Giles, A.B., 1984, MNRAS 208, 241

Eder, J., Lewis, B.M., Terzian, Y., 1988, ApJS 66, 183

Epchtein, N., Le Bertre, T., Lepine, J.R.D., 1990, A&A 227, 82

Faúndez-Abans, M., Maciel, W.J. 1986, Rev.Mex.Astronomia y Astrofisica 12, 240

Feast, M.W., Glass, I.S., Whitelock, P.A., Catchpole, R.M., 1989, MNRAS 241, 375

Fleming, T.A., Liebert, J., Green, R.F., 1986, ApJ 308, 176

Garwood, R., Jones, T.J., 1987, PASP 99, 453

Groenewegen, M.A.T., van den Hoek, L.B., de Jong, T., 1993, A&A 293, 381 (GHJ)

Groenewegen, M.A.T., de Jong, T., 1993, A&A 267, 410 (GJ)

Groenewegen, M.A.T., de Jong, T., 1994a, A&A 282, 127

Groenewegen, M.A.T., de Jong, T., 1994b, A&A 283, 463

Groenewegen, M.A.T., de Jong, T., 1994c, A&A 288, 782

Groenewegen, M.A.T., de Jong, T., van der Bliek, N.S., Slijkhuis, S., Willems, F.J., 1992, A&A 253, 150

Guglielmo, F. 1990, Publ. Obs. Paris

Guglielmo, F. 1993, Thesis, Université de Paris VII

Iben Jr., I., Renzini, A., 1983, ARAA 21, 271

Isaacman, R., 1983, in IAU Symp. 103, ed. D. R. Flower, Reidel, Dordrecht, p.415

Ivison, R.J., Seaquist, E.R., Hall, P.J., 1994, MNRAS 269, 218

Jura, M., 1994, ApJ 422, 102

Jura, M., Joyce, R.R., Kleinmann, S.G., 1989, ApJ 336, 924

Jura, M., Yamamoto, A., Kleinmann, S.G., 1993, ApJ 413, 298

Jura, M., Kleinmann, S.G., 1989, ApJ 341, 359

Jura, M., Kleinmann, S.G., 1992, ApJS 79, 105

Lépine, J.R.D., Ortiz, R., Epchtein, N., 1995, A&A (in press, LOE)

Le Squeren, A.M., Sivagnanam, P., Dennefeld, M., David, P., 1992, A&A 254, 133

Lewis, B.M., 1994, ApJS 93, 549

Lewis, B.M., Eder, J., Terzian, Y., 1990, ApJ 362, 634

Lewis, B.M., Engels, D., 1993, MNRAS 265, 161

Likkel, L., 1989, ApJ 344, 350

Maciel, W.J., 1981, A&A 98, 406

Maciel, W.J., 1989, in IAU Symposium , ed. S. Torres-Peimbert, p. 73

Maciel, W.J., Chiappini, C., 1994, Ap&SS 219, 231

Maciel, W.J., Dutra, C.M., 1992, A&A 262, 271 (MD)

Maciel, W.J., Köppen, J. 1994, A&A 282, 436

Matteucci, F., François, P., 1989, MNRAS 239, 885

Miller, G.E., Scalo, J.M., 1979, ApJS 41, 513

Neugebauer, G., Leighton, R.B., 1969, Two Micron Sky Survey, NASA SP-3047

Olnon, F.M., Baud, B., Habing, H.J., de Jong, T., Harris, S., Pottasch, S.R., 1984, ApJ 278, L41

Ortiz, R., Maciel, W.J., 1994, A&A 287, 552 (OM)

Ortiz, R., Lépine, J.R.D., 1993, A&A 279, 90 (OL)

Peimbert, M., 1978, in IAU Symposium 76, ed. Y.Terzian, Reidel, Dordrecht, p.215

Phillips, J.P., 1989, in IAU Symposium , ed. S. Torres-Peimbert, p.425

Pottasch, S.R., 1984, Planetary Nebulae, Reidel, Dordrecht

Pottasch, S.R., 1995, A&A (in press)

Reimers, D., 1975, in Problems in stellar atmospheres and envelopes, eds. B. Baschek, W.H. Kegel, G. Traving, Springer, Berlin, p.229

Renzini, A., 1981, in Physical processes in red giants, eds. I.Iben Jr., A. Renzini, Reidel, Dordrecht, p.431

Renzini, A., Voli, M., 1981, A&A 94, 175

Ruelas-Mayorga, R.A., 1991a, Rev.Mex.Astronomia y Astrofisica 22, 27

Ruelas-Mayorga, R.A., 1991b, Rev.Mex.Astronomia y Astrofisica 22, 43

Schoenberner, D., 1983, ApJ 272, 708

Seaquist, E.R., Ivison, R.J., 1994, MNRAS 269, 512

Shklovskii, I.S., 1956, Astr. Zhurnal 33, 315

Sivagnanam, P., Le Squeren, A.M., Foy, F., 1988, A&A 206, 285

te Lintel Hekkert, P., Versteege-Hensel, H.A., Habing, H.J., Wiertz, M., 1989, A&AS 78, 399

te Lintel Hekkert, P., 1990, Thesis, Leiden

te Lintel Hekkert, P., Caswell, J.L., Habing, H.J., Haynes, R.F., Norris, R.P., 1991, A&AS 90, 327

Tinsley, B.M., 1978, in IAU Symp. 76, ed. Y. Terzian, Reidel, Dordrecht, p. 341

van der Veen, W.E.C.J., 1988, PhD Thesis, Leiden

Vassiliadis, E., Wood, P.R., 1993, ApJ 413, 641 (VW)

Wainscoat, R.J., Cohen, M., Volk, K., Walker, H.J., Schwartz, D.E., 1992, ApJS 83, 111

Weidemann, V., 1991, White dwarfs, ed. G. Vauclair, E. M. Sion, Kluwer, Dordrecht, p. 230

Whitelock, P.A., Menzies, J., Feast, M., Marang, F., Carter, B., Roberts, G., Catchpole, R., Chapman, J., 1994, MNRAS 267, 711

Wilson, W.J., Barrett, A.H., 1968, AJ 73, 209

Wood, P.R., Cahn, J.H., 1977, ApJ 211, 499

Zijlstra, A.A., Pottasch, S.R., 1991, A&A 243, 478

Zuckerman, B., Aller, L.H., 1986, ApJ 301, 772

This article was processed by the author using Springer-Verlag TEX A&A macro package 1992.